Environmental Science & Technology Letters

pubs.acs.org/journal/estlcu

Letter

Evidence for Large Amounts of Brown Carbonaceous Tarballs in the Himalayan Atmosphere

Qi Yuan, Jianzhong Xu, Lei Liu, Aoxing Zhang, Yanmei Liu, Jian Zhang, Xin Wan, Mengmeng Li, Kai Qin, Zhiyuan Cong, Yuhang Wang, Shichang Kang, Zongbo Shi, Mihály Pósfai, and Weijun Li*

Cite This: *Environ. Sci. Technol. Lett.* 2021, 8, 16−23

Read Online

ACCESS | Metrics & More | Article Recommendations | Supporting Information

ABSTRACT: Primary brown carbon (BrC) co-emitted with black carbon (BC) from biomass burning is an important light-absorbing carbonaceous aerosol. BC from the Indo-Gangetic Plain can reach the Himalaya region and influence glacial melting and climatic change. However, to date, there is still not sufficient direct evidence for primary BrC in the Himalayan atmosphere. Here, we detected light-absorbing tarballs at microscopic scale collected on the northern slope of the Himalayas. We found that about 28% of thousands of individual particles were tarballs. The median sizes of externally mixed tarballs and internally mixed tarballs were 213 and 348 nm, respectively. Air mass trajectories, satellite detection, and Weather Research and Forecasting model coupled to Chemistry (WRF-Chem) simulations all indicated that these tarballs were emitted from biomass burning in the Indo-Gangetic Plain. A climate model simulation shows a significant heating effect (+0.01−4.06 W/m^2) of the tarballs in the Himalayan atmosphere. We conclude that the tarballs from long-range transport can be an important factor in the climatic effect and would correspond to a substantial influence on glacial melting in the Himalaya region.

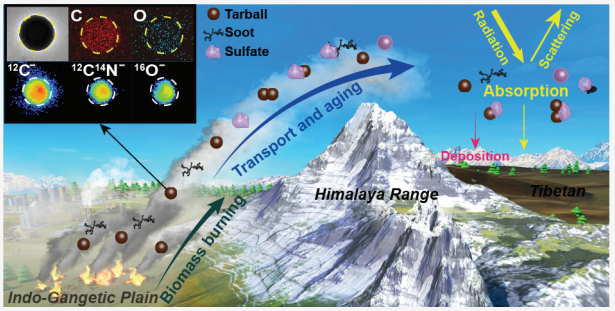

INTRODUCTION

The Himalaya−Tibetan Plateau (HTP), often referred to as the "third pole",[1] exhibits as the "Asian water tower" and plays a crucial role in supplying water for the Asian ecosystem and human survival owing to the largest reserves of glacial area (~10^5 km^2) beside the polar regions.[2] Over the past decade, the HTP glaciers have been retreating continuously, and the Himalayan glaciers have the greatest recession due to their extreme sensitivity to climate change and anthropogenic influence.[3] The long-range transport of light-absorbing carbonaceous particles by the Asian monsoon system could accelerate the melting of glaciers by deposition on the snow and ice surface.[4−6]

Brown carbon (BrC) is an important light-absorbing fine carbonaceous aerosol in addition to black carbon (BC).[7,8] BrC can modify the Asian monsoon rainfall, affect the hydrological cycle, and accelerate glacial melting.[9−11] Primary BrC from combustion is the major species of BrC and is usually co-emitted with BC during biomass burning.[8] However, previous literature mostly paid attention to BC in the Himalaya region,[6,12−15] and some studies reported secondary BrC.[16] To date, few studies have provided sufficient direct evidence of primary BrC in the Himalayan atmosphere.[17,18] The main challenge is to reliably identify the primary BrC subcategory of carbonaceous aerosol by using online/filter-based bulk measurements, including aerosol mass spectrometry[19,20] and single particle soot photometry,[21] especially in the clean Himalayan atmosphere with low concentrations of carbonaceous aerosol (mostly <5 μg/m^3).[15] If primary BrC particles occur in the Himalayan atmosphere, as is probable, they must influence atmospheric optical properties and contribute to the glacier retreating problem alongside BC and secondary BrC.[6,16] Tarball is a polymerized, particular, and abundant particle type of primary BrC with a spherical shape, a small size, a high viscosity, and an insoluble amorphous property.[21−23] Tarball is mainly emitted from fossil fuel burning or biomass burning and formed by the chemical or thermal transformation of low-molecular-weight organic molecules.[21] Tarball consists of major C, O, and N, with minor S and K.[21−23] On the basis of their refractory properties, spherical shapes, and small sizes, tarballs can be identified by electron microscopy.[22,24,25]

Here, we have attempted to use various electron microscopy analyses to identify primary BrC through ground-based sampling at the Qomolangma Station (QOMS), a remote site at high altitude along the northern slope of the Himalayas.

Received: September 14, 2020
Revised: October 20, 2020
Accepted: October 20, 2020
Published: November 4, 2020

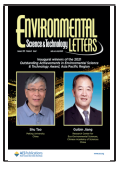

https://dx.doi.org/10.1021/acs.estlett.0c00735
Environ. Sci. Technol. Lett. 2021, 8, 16−23

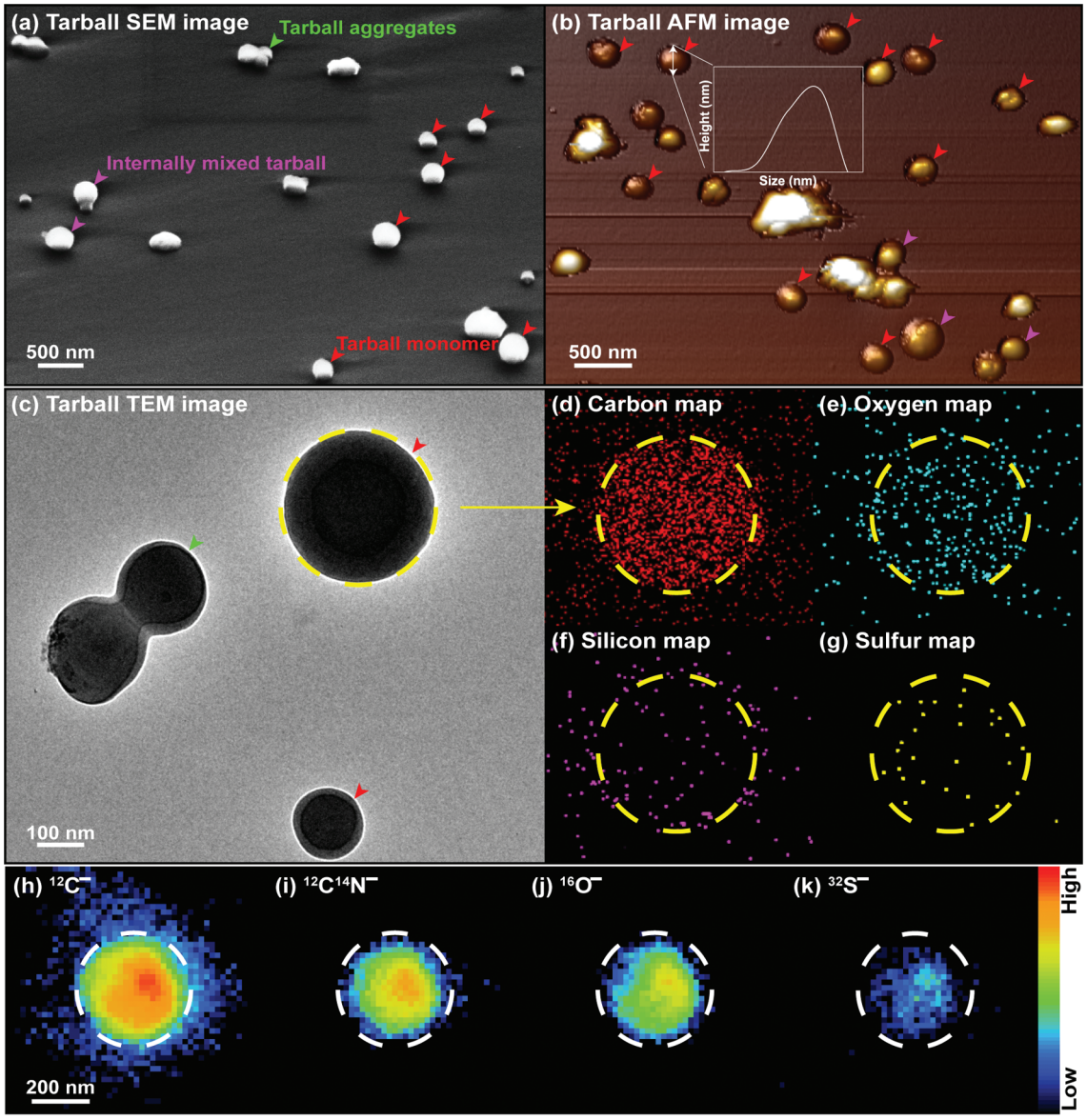

Figure 1. Microscope images of tarballs. (a) SEM image at 60° tilt angle of tarballs. (b)AFM image of tarballs. (c) TEM bright-field image of tarballs. (d–g) TEM-EDS elemental maps of C, O, Si, and S of a tarball monomer. (h–k) NanoSIMS ion intensity maps of $^{12}C^-$, $^{16}O^-$, $^{12}C^{14}N^-$, and $^{32}S^-$ of a tarball monomer.

This remote site locates in a desolate environment with rare vegetation and harsh weather conditions.[26] The air pollutants from the Indo-Gangetic Plain can cross Mt. Everest and reach QOMS via the westerly synoptic-scale circulation[13] and mountain–valley wind,[27] suggesting that QOMS is a suitable site for studying the evidence for long-range transport of anthropogenic aerosols. Air mass backward trajectories, satellite data, and the Weather Research and Forecasting model coupled to Chemistry (WRF-Chem) were used to trace their possible transport paths. Our findings provide direct evidence for primary BrC from the Indo-Gangetic Plain being transported into the Himalayan atmosphere in the premonsoon season.

MATERIALS AND METHODS

Sampling Site and Bulk Measurement. Our field observation was conducted from 23 April to 4 May in 2016, at the background QOMS (86.95° E, 28.36° N; 4276 m a.s.l.) on the north slope of the Himalayas and at the toe of Mt. Everest (Figure S1). The QOMS locates in a long valley covered by a group of glaciers at higher elevations, and strong mountain–valley winds are produced.[26] This background site is far from human activities, and the nearest densely inhabited district (Dingri County with a population of ~10^4) is approximately 100 km to the north. An Aerodyne high-resolution time-of-flight aerosol mass spectrometer (HR-ToF-AMS, Aerodyne Research Inc., Billerica, MA, USA) was used to measure the chemical compositions (organics, sulfate et al.) of submicrometer particles at the QOMS.[15] According to the HR-ToF-AMS observation, we divided our sampling period into two typical events: polluted days (25–30 April, PM_1: 9.0 $\mu g/m^3$) and clean days (23–24 April and 1–4 May, PM_1: 2.9 $\mu g/m^3$) (Figures S2 and S3). More details of the bulk measurements are included in the Text S1.

Individual Particle Collection and Microscopic Analysis. The individual particle samples were collected according

https://dx.doi.org/10.1021/acs.estlett.0c00735
Environ. Sci. Technol. Lett. 2021, 8, 16–23

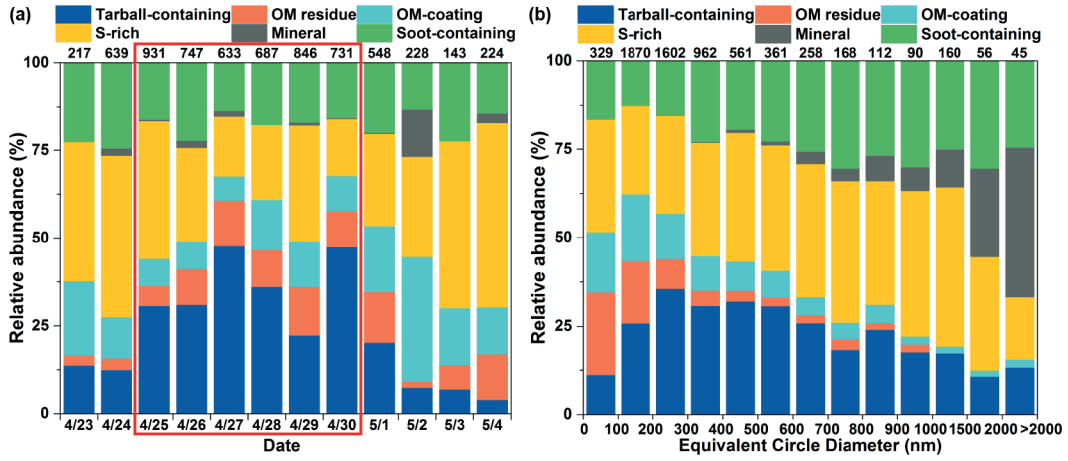

Figure 2. Relative abundances of six major particle types in this observation. (a) Relative abundances of individual particles from 23 April to 4 May, 2016. (b) Relative abundances of individual particles in different size ranges. A total of 6574 particles were analyzed, and the number of analyzed particles is shown above the column. The red frame in the left panel contains polluted days influenced by westerly or southwesterly winds.

to the detailed procedures in Text S2 and Yuan et al.[28] A scanning electron microscope (SEM, Zeiss Ultra 55, Germany), an atomic force microscope (AFM, Dimension Icon, Veeco Instruments Inc., USA), a transmission electron microscope (TEM, JEOL JEM-2100, Japan) combined with an energy-dispersive X-ray spectroscopy (EDS, INCA X-Max^N 80T, Oxford Instruments, UK), and a nanoscale secondary ion mass spectrometer 50L (NanoSIMS, CAMECA Instruments, Geneviers, France) were employed to systematically characterize the morphology, size, composition, and mixing state of tarballs in the samples. Further details of the microscope analyses can be found in Text S3 and Li et al.[29]

Backward Trajectory, Fire Spot Information, and CALIPSO Data Analysis. The 72-h backward trajectories were calculated every 2 h and clustered for each day at an ending height of 50 m above ground level by using a Hybrid Single Particle Lagrange Integrated Trajectory (HYSPLIT). Various active fire spots were detected over South and Southeast Asia by the Fire Information for Resource Management System (FIRMS) provided by the MODIS satellite (https://firms.modaps.eosdis.nasa.gov). Cloud-Aerosol Lidar and Infrared Pathfinder Satellite Observation (CALIPSO) provides a direct measurement of the aerosol subtype (http://www-calipso.larc.nasa.gov/).

WRF-Chem Model Simulation. The WRF-Chem model (version 4.1) has been proved to be an effective transport model with a combination of meteorological and chemical factors[30,31] and is widely implied for simulating the carbonaceous aerosols emission and transport in South Asia and the HTP.[32] In this study, the WRF-Chem simulated the surface mass concentrations of organic carbon (OC) and BC and the regional wind fields in South Asia and the southern HTP from 08:00 (Beijing time) on 1 April to 07:00 (Beijing time) on 1 June, 2016. Further details can be found in Text S4.

Hygroscopicity Measurements. An individual particle hygroscopic (IPH) system was built to observe the hygroscopic properties of tarballs at different relative humidity (RH) values. This IPH system has successfully captured the hygroscopic growth of individual particles collected on either a silicon wafer or TEM grid.[33] In this study, two typical samples were chosen to observe the hygroscopic growth of tarballs at RHs ranging from 10% to 85%.

Optical Properties Calculation and Direct Radiative Effect Simulation. The absorption cross section (ACS) values of sulfate-mixed tarball (named tarball-S) particles with core−shell structures and those of tarball cores are calculated by using the BHCOAT code.[34] For calculation, the refractive index of the sulfate coating was set to m = 1.55−0.00i at 550 nm, and a refractive index of 1.84−0.21i at 550 nm[25] was used for the tarball core. The Santa Barbara DISORT Atmospheric Radiative Transfer (SBDART) model[35] was used to investigate the direct radiative effect (DRE) of tarballs and BC in a short wave range (0.25−1.05 μm) at the top of the QOMS atmosphere during the sampling period. The various refractive index and absorption Ångström exponent values of tarballs in previous studies were used for DRE simulation.[24,25,36−38] Further details can be found in Text S5.

RESULTS AND DISCUSSION

Relative Abundance and Source of Tarballs. Electron microscopy analysis generally shows that large numbers of fine spherical particles occur in the samples (Figure 1a−c). EDS shows that they mainly consist of C with minor O, Si, S, and K. Elemental mapping of these fine spherical particles shows that they contain abundant C and minor O, Si, and S distributed throughout the particles (Figure 1d−g). NanoSIMS analysis produces strong signals and uniform distributions of $^{12}C^-$, $^{16}O^-$, and $^{12}C^{14}N^-$ and a bit weaker signal of $^{32}S^-$, thus confirming that this type of particle consists of organic matter (Figure 1h−k). The spherical organic particles with a high viscosity are likely primary particles emitted from combustion sources[39] and are identified as tarballs in the atmosphere.[7,22,23,40] SEM images taken at a sample stage tilt of 60° and AFM images both show that the tarballs still maintain spherical shapes after impacting on the substrate (Figure 1a, b). These results suggest that tarballs should be in a glassy solid state in the atmosphere.[22] In the following, we define individual particles containing tarballs as tarball-containing particles.

Unexpectedly, tarball-containing particles accounted for an average of 28% (±18%, variability between samples) by number of the total analyzed particles, which was higher than the observation result (3%) of Cong et al.,[17] indicating a more significant anthropogenic interference at the background QOMS during the sampling period. The contribution of

https://dx.doi.org/10.1021/acs.estlett.0c00735
Environ. Sci. Technol. Lett. 2021, 8, 16−23

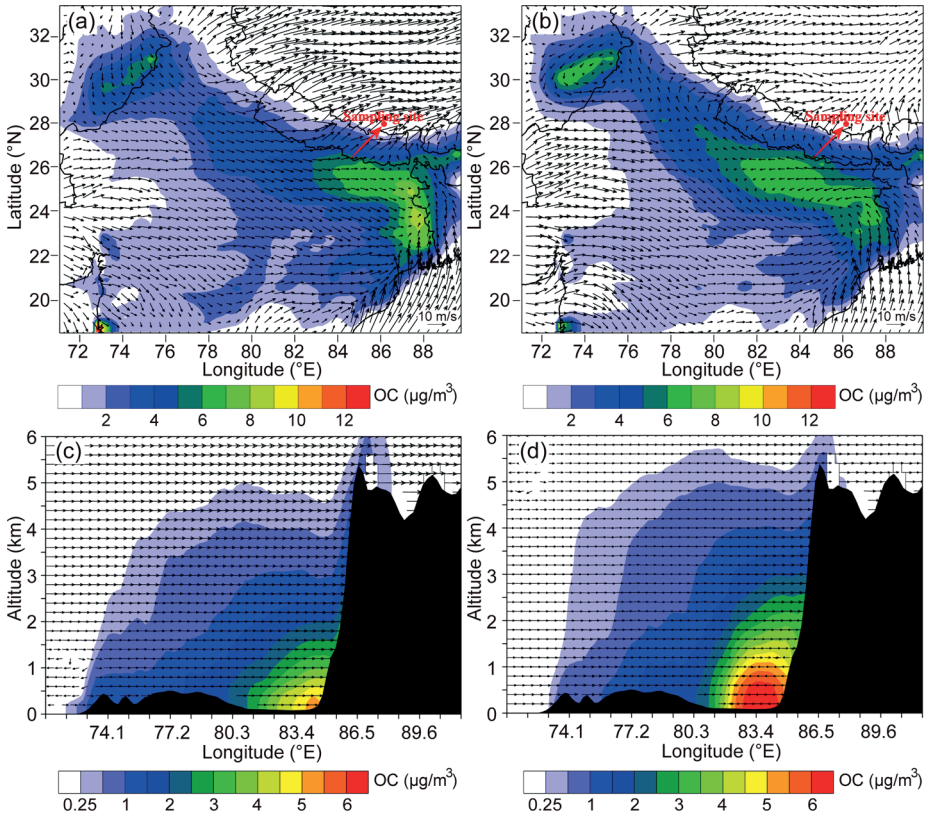

Figure 3. Horizontal and vertical distributions of OC and wind fields in South Asia and southern HTP. (a) Simulated horizontal spatial distributions of surface OC concentrations and winds at 12:00−20:00 (Beijing time) in April 2016. (b) Simulated horizontal spatial distributions of surface OC concentrations and winds at 12:00−20:00 (Beijing time) in May 2016. (c) Vertical profiles of OC concentration and winds at 12:00−20:00 (Beijing time) in April 2016. (d)Vertical profiles of OC concentration and winds at 12:00−20:00 (Beijing time) in May 2016. The red circle dot (a, b) represents the sampling site. The orientations of the black arrows (a−d) refer to the wind direction, and the lengths of the black arrows refer to the wind speed. Scale bars (a−d) show the mass concentrations of OC. The thick red arrows (a, b) represent the upward transport from the Indo-Gangetic Plain to the HTP. Air along the mountain face flows out of the image toward the viewer (Figures S6 and S7). The line used for the cross section of the vertical WRF-Chem simulation can be seen in Figure S6. The black color (c, d) indicates the profile of the Himalaya Mountains.

tarball-containing particles to the total particle counts increased from 12% on clean days to 38% on polluted days, with the highest value of 53% occurring on 27 April (Figure 2a, Figures S4 and S5). Tarball-containing particles occurred in the fine mode, and 80% of them were smaller than 500 nm (Figure 2b). Furthermore, HR-ToF-AMS measurements showed that organic aerosols were the dominant PM_1 species (contributing 51% ± 8% on average to the total PM_1 mass) during the sampling period, and biomass burning organic aerosol (BBOA) contributed a large fraction (36.6%) to the total organic aerosol mass (Figure S2). The mass concentrations of BBOA and BC at the QOMS increased from 0.76 and 0.92 $\mu g/m^3$ on clean days to 1.78 and 2.01 $\mu g/m^3$ on polluted days, respectively (Figure S2). In brief, our results provide direct evidence that large numbers of tarballs occurred in the Himalayan atmosphere during the sampling period.

The 72-h backward trajectories showed that westerly and southwesterly air masses were the dominant sources of aerosol particles during 23−30 April and passed through Pakistan, India, and Nepal before arriving at the QOMS (Figure S1). The average fraction of tarball-containing particles was 34% when the westerly and southwesterly air masses prevailed. During the dominance of easterly and northerly air masses, the fraction of tarball-containing particles decreased to 11%, and the fraction of mineral particles increased 7 times (Figures S1 and S5). MODIS data further showed that a dense array of active fire spots occurred along the pathways of westerly air masses (Figure S1). In the Indo-Gangetic Plain, large-scale wheat-residue burning is the principle source of biomass burning emissions, after the wheat crops are harvested in April−May each year.[41,42] Wheat residue burning can emit large amounts of spherical organic particles with a small amount of soot particles.[39] Satellite and ground-based laser radar observations both have proved that biomass burning smoke can be injected into the stratosphere, and light-absorbing aerosols could promote the rising smoke plumes due to solar heating.[43] Here, the horizontal WRF-Chem simulation shows that the ground southwesterly wind at noon and the afternoon of each day brought high concentrations of air pollutants from the Indo-Gangetic Plain to the south of the Himalayas during the entire April and May (Figure 3, Figures S6 and S7). The vertical WRF-Chem simulation also shows that the southwesterly wind prevailing at a 1−6 km height lifted a small part of the carbonaceous aerosols from the high emission zone in the low central Indo-Gangetic Plain to the high Himalayas (Figure 3, Figures S6 and S7). Furthermore, the CALIPSO data shows that a thick air pollutant layer containing large amounts of smoke aerosols from the Indo-Gangetic Plain climbed along the south ridge of the Himalayas into the Tibetan plateau following the elevated air masses

https://dx.doi.org/10.1021/acs.estlett.0c00735
Environ. Sci. Technol. Lett. 2021, 8, 16−23

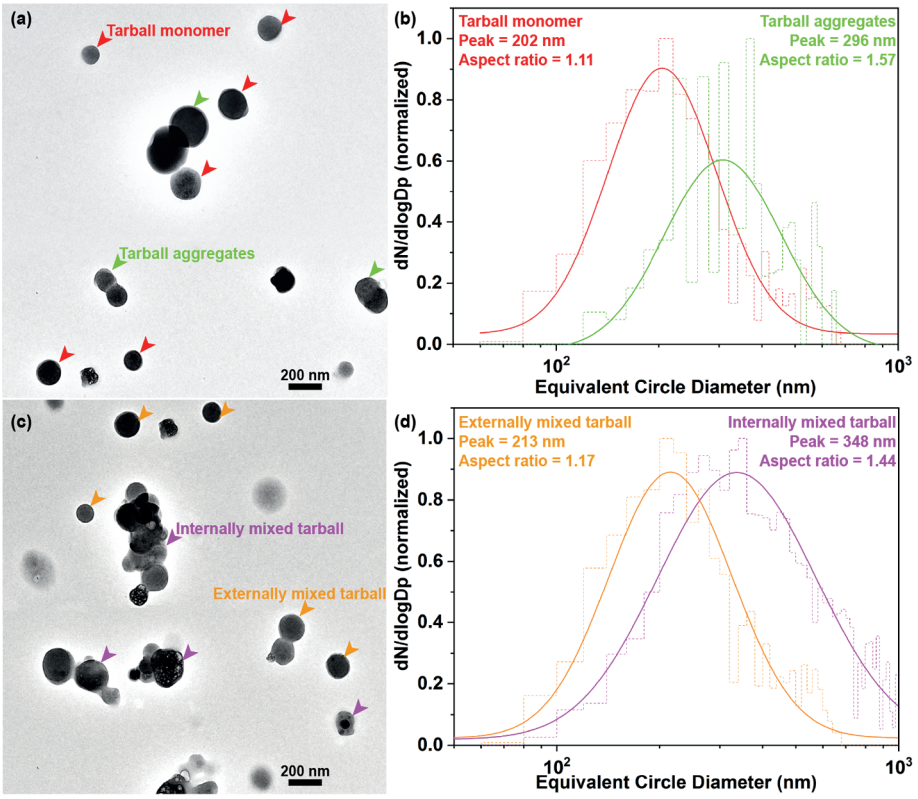

Figure 4. Shapes and size distributions of tarball-containing particles. (a) TEM image of tarball monomers and tarball aggregates. (b) Size distributions of tarballs monomers and tarball aggregates. The log-normal peaks are at 202 nm (σ = 2.3) and 296 nm (σ = 2.5) for tarball monomers and tarball aggregates, respectively. (c) TEM image of externally and internally mixed tarballs. (d) Size distributions of externally and internally mixed tarballs. The log-normal peaks are at 213 nm (σ = 2.6) and 348 nm (σ = 3.4) for externally and internally mixed tarballs, respectively.

(Figure S8). In this study, the air mass backward trajectories, CALIPSO data, WRF-Chem simulation, and field investigations are all consistent with the interpretation that the tarball-containing particles observed in the Himalaya region were sourced from agricultural residue burning in the Indo-Gangetic Plain. Indeed, a few previous studies suggested that air pollutants from the Indo-Gangetic Plain can be elevated along the south slope of the Himalayas and transported further into the Tibetan Plateau in the premonsoon season.[15,17,27,44,45]

Size Distributions, Mixing States, and Aging of Tarballs. On the basis of the characteristic morphology of tarballs, we identify tarball monomers and tarball aggregates (Figure 4a, c). Tarball monomers are isolated spherical particles with a low aspect ratio of nearly 1 (Figure S9, a mean aspect ratio of 1.11). The tarball aggregates appear as agglomerates of two or more tarball monomers (Figure 4a, c), and they show various irregular shapes with a relatively high aspect ratio (Figure S9, a mean aspect ratio of 1.57). Figure 4b shows that the size distribution of tarball aggregates displays a peak at 296 nm (geometric standard deviation, σ = 2.5), whereas the peak for tarball monomers occurs at 202 nm (σ = 2.3). Model simulation shows that the lifetime of BC from India is approximately 5 days,[46] and their spherical geometry could increase the lifetime of aerosols compared with fractal agglomerates.[47,48] Tarballs exhibit a similar small size and hydrophobic property but more spherical morphology by comparing with BC. Therefore, like BC, tarballs from the Indo-Gangetic Plain could be transported long distances to the Himalayan atmosphere.

On the basis of the mixing state of individual particles, we distinguished externally mixed (only tarball) and internally mixed tarballs (tarball associated with other aerosols) (Figure 4c). Approximately 43% of all tarball-containing particles during the sampling period were externally mixed tarballs, while the rest were tarball-S particles (Figure 4c and Figure S10a). The size distribution of externally mixed tarballs peaked at 213 nm (σ = 2.6), which is consistent with the results of the other observations,[22,23] and occurred at a much smaller value than the peak at 348 nm (σ = 3.4) for internally mixed tarballs (Figure 4d). This result suggests that secondary sulfate mixed with the tarballs increased particle size (Figure S10b, d). Hygroscopic experiments with individual particles further showed that the externally mixed tarballs had extremely weak hygroscopicity under RH = 85%, whereas the aged tarballs mixed with sulfates started to take up water at RH = 65% with a mean growth factor of 1.3−1.4 at RH = 85% (Figure S11). Here, we can infer that atmospheric aging via sulfate coating favors the hygroscopic growth of tarballs during long-range transport.

Optical Property and Climatic Effect of Tarballs in the HTP. The Himalaya region has an extremely high altitude and is the most vulnerable region on the planet aside from the south and north poles.[1,49] Compared with other places in the world, anthropogenic aerosols from outside the Himalaya region could trigger various climate and environment problems.[5,50] Our observations conducted at a high-elevation background site of the Himalaya provided direct evidence of abundant tarballs occurring there. Intense agricultural biomass

https://dx.doi.org/10.1021/acs.estlett.0c00735
Environ. Sci. Technol. Lett. 2021, 8, 16−23

burning activities in the Indo-Gangetic Plain during the premonsoon season[51] contributed abundant primary BrC beside BC into the Himalayan atmosphere (Figure 2 and Figure S5).

Previous studies have shown that internal mixtures of BrC can enhance optical absorption by up to 70%, especially in the ultraviolet and short-visible range of the spectrum.[52,53] In our study, during the premonsoon season, approximately 28% of all particles were tarball-containing particles in the Himalayan atmosphere, and approximately one-third of internally mixed tarballs were found to be mixtures of a tarball core and a sulfate coating (Figure S10). A modeling calculation for tarball-S particles with core−shell mixing structures shows that a sulfate coating could increase the ACS of tarball-S particles on average by a factor of 2 compared to bare tarball cores (Figure S12). On the basis of this estimation, the tarballs internally mixed with sulfate shells would significantly increase optical absorption relative to the externally mixed tarballs. Once these abundant atmospheric tarball-containing particles are deposited onto the glacial surfaces of the Himalayas through either dry or wet deposition (Figure S13), their light absorption could intensify glacial melting.[54,55] The SBDART model simulation shows that the DRE of tarballs ranged between +0.01 and +4.06 W/m^2 (Table S1), which is lower than that of soot (+3.46−8.34 W/m^2) in the QOMS atmosphere (Table S2). As a result, the positive DRE values indicate that tarballs as the BrC contribute a significant warming effect to the QOMS atmosphere after BC. Consequently, the current climate models need to consider the long-range transport of primary tarballs on a regional scale in the future.

In summary, the present study demonstrates the significant impacts of seasonal agriculture biomass burning practices in the Indo-Gangetic Plain on the Himalayan atmosphere (Figure S13). The present evidence of tarballs will promote the future evaluation of climatic and glacial effects of BrC in the Himalaya region.

■ ASSOCIATED CONTENT

Supporting Information

The Supporting Information is available free of charge at https://pubs.acs.org/doi/10.1021/acs.estlett.0c00735.

Additional text for the detailed information on bulk measurement (Text S1), individual particle collection (Text S2), microscope analysis of particles (Text S3), WRF-Chem simulation (Text S4), and DRE simulation (Text S5). Location of QOMS, 72-h backward trajectories and fire spots in the Indo-Gangetic Plain (Figure S1); time series of pollutants mass concentrations and weather conditions (Figure S2); pictures of the sampling site (Figure S3); TEM images of six major individual particle types (Figure S4); relative abundances of individual particles at each sampling time (Figure S5); line used for the cross section of the vertical WRF-Chem simulation (Figure S6); horizontal and vertical simulation of BC and wind fields in the South Asia and southern HTP (Figure S7); CALIPSO aerosol subtype of ground tracks (Figure S8); aspect ratio of tarball monomers and tarball aggregates (Figure S9); relative abundances, TEM images, and EDS spectrum of two typical internally mixed tarballs (Figure S10); deliquescent processes of particles as a function of RH (Figure S11); box-and-scatter point overlap plot showing the ratio of ACS of tarball-S particles with core−shell structures to ACS of tarball cores (Figure S12); and conceptual model illustrating the transports and radiation effects of tarballs (Figure S13). DRE of tarballs (Table S1) and soot (Table S2) in the QOMS atmosphere during the sampling period. (PDF)

■ AUTHOR INFORMATION

Corresponding Author

Weijun Li − *Key Laboratory of Geoscience Big Data and Deep Resource of Zhejiang Province, Department of Atmospheric Sciences, School of Earth Sciences, Zhejiang University, Hangzhou 310027, China;* orcid.org/0000-0003-4887-4260; Email: liweijun@zju.edu.cn

Authors

Qi Yuan − *Key Laboratory of Geoscience Big Data and Deep Resource of Zhejiang Province, Department of Atmospheric Sciences, School of Earth Sciences, Zhejiang University, Hangzhou 310027, China*

Jianzhong Xu − *State Key Laboratory of Cryospheric Sciences, Northwest Institute of Eco-Environment and Resources, Chinese Academy of Sciences (CAS), Lanzhou 730000, China;* orcid.org/0000-0002-9933-1744

Lei Liu − *Key Laboratory of Geoscience Big Data and Deep Resource of Zhejiang Province, Department of Atmospheric Sciences, School of Earth Sciences, Zhejiang University, Hangzhou 310027, China;* orcid.org/0000-0002-7171-1454

Aoxing Zhang − *School of Earth and Atmospheric Sciences, Georgia Institute of Technology, Atlanta, Georgia 30332, United States*

Yanmei Liu − *State Key Laboratory of Cryospheric Sciences, Northwest Institute of Eco-Environment and Resources, Chinese Academy of Sciences (CAS), Lanzhou 730000, China*

Jian Zhang − *Key Laboratory of Geoscience Big Data and Deep Resource of Zhejiang Province, Department of Atmospheric Sciences, School of Earth Sciences, Zhejiang University, Hangzhou 310027, China*

Xin Wan − *Institute of Tibetan Plateau Research, CAS, Beijing 100101, China*

Mengmeng Li − *School of Atmospheric Sciences, CMA-NJU Joint Laboratory for Climate Prediction Studies, Jiangsu Collaborative Innovation Center for Climate Change, Nanjing University, Nanjing 210023, China*

Kai Qin − *School of Environment and Geoinformatics, China University of Mining and Technology, Xuzhou 221116, China*

Zhiyuan Cong − *Institute of Tibetan Plateau Research, CAS, Beijing 100101, China;* orcid.org/0000-0002-7545-5611

Yuhang Wang − *School of Earth and Atmospheric Sciences, Georgia Institute of Technology, Atlanta, Georgia 30332, United States;* orcid.org/0000-0002-7290-2551

Shichang Kang − *State Key Laboratory of Cryospheric Sciences, Northwest Institute of Eco-Environment and Resources, Chinese Academy of Sciences (CAS), Lanzhou 730000, China; CAS Center for Excellence in Tibetan Plateau Earth Sciences, Beijing 100101, China*

Zongbo Shi − *School of Geography, Earth and Environmental Sciences, University of Birmingham, Birmingham B15 2TT, United Kingdom;* orcid.org/0000-0002-7157-543X

Mihály Pósfai − *Department of Earth and Environmental Sciences, University of Pannonia, Veszprém H8200, Hungary*

https://dx.doi.org/10.1021/acs.estlett.0c00735
Environ. Sci. Technol. Lett. 2021, 8, 16−23

Complete contact information is available at:
https://pubs.acs.org/10.1021/acs.estlett.0c00735

Notes

The authors declare no competing financial interest.

■ ACKNOWLEDGMENTS

The authors are grateful to Ms. Jianwei Chi for her assistance in sample collection. We appreciate Peter Hyde's comments and proofreading. This work was funded by the National Natural Science Foundation of China (42075096, 41805099), China Postdoctoral Science Foundation (2018M632449), Research Funding of School of Earth Sciences of Zhejiang University and Hundred Talents Program in Zhejiang University, second Tibetan Plateau Scientific Expedition and Research Program (STEP) (2019QZKK0605).

■ REFERENCES

(1) Qiu, J. The third pole. *Nature* **2008**, *454* (7203), 393−396.
(2) Immerzeel, W. W.; van Beek, L. P. H.; Bierkens, M. F. P. Climate change will affect the Asian Water Towers. *Science* **2010**, *328* (5984), 1382−1385.
(3) Yao, T. D.; Thompson, L.; Yang, W.; Yu, W. S.; Gao, Y.; Guo, X. J.; Yang, X. X.; Duan, K. Q.; Zhao, H. B.; Xu, B. Q.; Pu, J. C.; Lu, A. X.; Xiang, Y.; Kattel, D. B.; Joswiak, D. Different glacier status with atmospheric circulations in Tibetan Plateau and surroundings. *Nat. Clim. Change* **2012**, *2* (9), 663−667.
(4) Ramanathan, V.; Carmichael, G. Global and regional climate changes due to black carbon. *Nat. Geosci.* **2008**, *1* (4), 221−227.
(5) Alvarado, M. J.; Winijkul, E.; Adams-Selin, R.; Hunt, E.; Brodowski, C.; Lonsdale, C. R.; Shindell, D. T.; Faluvegi, G.; Kleiman, G.; Mosier, T. M.; Kumar, R. Sources of Black Carbon Deposition to the Himalayan Glaciers in Current and Future climates. *J. Geophys. Res.- Atmos.* **2018**, *123* (14), 7482−7505.
(6) Li, C. L.; Bosch, C.; Kang, S. C.; Andersson, A.; Chen, P. F.; Zhang, Q. G.; Cong, Z. Y.; Chen, B.; Qin, D. H.; Gustafsson, O. Sources of black carbon to the Himalayan-Tibetan Plateau glaciers. *Nat. Commun.* **2016**, *7*, 7.
(7) Laskin, A.; Laskin, J.; Nizkorodov, S. A. Chemistry of atmospheric brown carbon. *Chem. Rev.* **2015**, *115* (10), 4335−4382.
(8) Saleh, R.; Robinson, E. S.; Tkacik, D. S.; Ahern, A. T.; Liu, S.; Aiken, A. C.; Sullivan, R. C.; Presto, A. A.; Dubey, M. K.; Yokelson, R. J.; Donahue, N. M.; Robinson, A. L. Brownness of organics in aerosols from biomass burning linked to their black carbon content. *Nat. Geosci.* **2014**, *7* (9), 647−650.
(9) Xu, J. Z.; Zhang, Q.; Li, X. Y.; Ge, X. L.; Xiao, C. D.; Ren, J. W.; Qin, D. H. Dissolved Organic Matter and Inorganic Ions in a Central Himalayan Glacier-Insights into Chemical Composition and Atmospheric Sources. *Environ. Sci. Technol.* **2013**, *47* (12), 6181−6188.
(10) Chu, J. E.; Kim, K. M.; Lau, W. K. M.; Ha, K. J. How light-absorbing properties of organic aerosol modify the Asian summer monsoon rainfall? *J. Geophys. Res.- Atmos.* **2018**, *123* (4), 2244−2255.
(11) Ramanathan, V.; Crutzen, P. J.; Kiehl, J. T.; Rosenfeld, D. Atmosphere - Aerosols, climate, and the hydrological cycle. *Science* **2001**, *294* (5549), 2119−2124.
(12) Kopacz, M.; Mauzerall, D. L.; Wang, J.; Leibensperger, E. M.; Henze, D. K.; Singh, K. Origin and radiative forcing of black carbon transported to the Himalayas and Tibetan Plateau. *Atmos. Chem. Phys.* **2011**, *11* (6), 2837−2852.
(13) Chen, X. T.; Kang, S. C.; Cong, Z. Y.; Yang, J. H.; Ma, Y. M. Concentration, temporal variation, and sources of black carbon in the Mt. Everest region retrieved by real-time observation and simulation. *Atmos. Chem. Phys.* **2018**, *18* (17), 12859−12875.
(14) Marinoni, A.; Cristofanelli, P.; Laj, P.; Duchi, R.; Calzolari, F.; Decesari, S.; Sellegri, K.; Vuillermoz, E.; Verza, G. P.; Villani, P.; Bonasoni, P. Aerosol mass and black carbon concentrations, a two year record at NCO-P (5079 m, Southern Himalayas). *Atmos. Chem. Phys.* **2010**, *10* (17), 8551−8562.
(15) Zhang, X. H.; Xu, J. Z.; Kang, S. C.; Liu, Y. M.; Zhang, Q. Chemical characterization of long-range transport biomass burning emissions to the Himalayas: insights from high-resolution aerosol mass spectrometry. *Atmos. Chem. Phys.* **2018**, *18* (7), 4617−4638.
(16) Kirillova, E. N.; Marinoni, A.; Bonasoni, P.; Vuillermoz, E.; Facchini, M. C.; Fuzzi, S.; Decesari, S. Light absorption properties of brown carbon in the high Himalayas. *J. Geophys. Res.- Atmos.* **2016**, *121* (16), 9621−9639.
(17) Cong, Z.; Kang, S.; Dong, S.; Liu, X.; Qin, D. Elemental and individual particle analysis of atmospheric aerosols from high Himalayas. *Environ. Monit. Assess.* **2010**, *160* (1−4), 323−35.
(18) Yuan, Q.; Wan, X.; Cong, Z.; Li, M.; Liu, L.; Shu, S.; Liu, R.; Xu, L.; Zhang, J.; Ding, X.; Li, W. In Situ Observations of Light-Absorbing Carbonaceous Aerosols at Himalaya: Analysis of the South Asian Sources and Trans-Himalayan Valleys Transport Pathways. *J. Geophys. Res.: Atmos.* **2020**, *125* (18), No. e2020JD032615.
(19) Adachi, K.; Sedlacek, A. J.; Kleinman, L.; Chand, D.; Hubbe, J. M.; Buseck, P. R. Volume changes upon heating of aerosol particles from biomass burning using transmission electron microscopy. *Aerosol Sci. Technol.* **2018**, *52* (1), 46−56.
(20) Andreae, M. O.; Gelencsér, A. Black carbon or brown carbon? The nature of light-absorbing carbonaceous aerosols. *Atmos. Chem. Phys.* **2006**, *6*, 3131−3148.
(21) Corbin, J. C.; Gysel-Beer, M. Detection of tar brown carbon with a single particle soot photometer (SP2). *Atmos. Chem. Phys.* **2019**, *19* (24), 15673−15690.
(22) Adachi, K.; Sedlacek, A. J.; Kleinman, L.; Springston, S. R.; Wang, J.; Chand, D.; Hubbe, J. M.; Shilling, J. E.; Onasch, T. B.; Kinase, T.; Sakata, K.; Takahashi, Y.; Buseck, P. R. Spherical tarball particles form through rapid chemical and physical changes of organic matter in biomass-burning smoke. *Proc. Natl. Acad. Sci. U. S. A.* **2019**, *116* (39), 19336−19341.
(23) Pósfai, M.; Gelencsér, A.; Simonics, R.; Arató, K.; Li, J.; Hobbs, P. V.; Buseck, P. R. Atmospheric tar balls: particles from biomass and biofuel burning. *J. Geophys. Res.- Atmos.* **2004**, *109* (D6), 9.
(24) Hand, J. L.; Malm, W. C.; Laskin, A.; Day, D.; Lee, T.; Wang, C.; Carrico, C.; Carrillo, J.; Cowin, J. P.; Collett, J.; Iedema, M. J. Optical, physical, and chemical properties of tar balls observed during the Yosemite Aerosol Characterization Study. *J. Geophys. Res.* **2005**, *110* (D21), 14.
(25) Hoffer, A.; Tóth, A.; Nyirö-Kósa, I.; Pósfai, M.; Gelencsér, A. Light absorption properties of laboratory-generated tar ball particles. *Atmos. Chem. Phys.* **2016**, *16* (1), 239−246.
(26) Ma, Y. M.; Kang, S. C.; Zhu, L. P.; Xu, B. Q.; Tian, L. D.; Yao, T. D. Tibetan observation and research platform atmosphere-land interaction over a heterogeneous landscape. *Bull. Am. Meteorol. Soc.* **2008**, *89* (10), 1487−1492.
(27) Cong, Z. Y.; Kang, S. C.; Kawamura, K.; Liu, B.; Wan, X.; Wang, Z.; Gao, S.; Fu, P. Carbonaceous aerosols on the south edge of the Tibetan Plateau: concentrations, seasonality and sources. *Atmos. Chem. Phys.* **2015**, *15* (3), 1573−1584.
(28) Yuan, Q.; Xu, J.; Wang, Y.; Zhang, X.; Pang, Y.; Liu, L.; Bi, L.; Kang, S.; Li, W. Mixing State and Fractal Dimension of Soot Particles at a Remote Site in the Southeastern Tibetan Plateau. *Environ. Sci. Technol.* **2019**, *53* (14), 8227−8234.
(29) Li, W. J.; Xu, L.; Liu, X. H.; Zhang, J. C.; Lin, Y. T.; Yao, X. H.; Gao, H. W.; Zhang, D. Z.; Chen, J. M.; Wang, W. X.; Harrison, R. M.; Zhang, X. Y.; Shao, L. Y.; Fu, P. Q.; Nenes, A.; Shi, Z. B. Air pollution-aerosol interactions produce more bioavailable iron for ocean ecosystems. *Sci. Adv.* **2017**, *3* (3), e1601749.
(30) Grell, G. A.; Peckham, S. E.; Schmitz, R.; McKeen, S. A.; Frost, G.; Skamarock, W. C.; Eder, B. Fully coupled "online" chemistry within the WRF model. *Atmos. Environ.* **2005**, *39* (37), 6957−6975.
(31) Li, M.; Wang, T.; Xie, M.; Li, S.; Zhuang, B.; Huang, X.; Chen, P.; Zhao, M.; Liu, J. Formation and Evolution Mechanisms for Two Extreme Haze Episodes in the Yangtze River Delta Region of China

During Winter 2016. *J. Geophys. Res.: Atmos.* **2019**, *124* (6), 3607−3623.
(32) Gogoi, M. M.; Babu, S. S.; Moorthy, K. K.; Bhuyan, P. K.; Pathak, B.; Subba, T.; Chutia, L.; Kundu, S. S.; Bharali, C.; Borgohain, A.; Guha, A.; De, B. K.; Singh, B.; Chin, M. Radiative effects of absorbing aerosols over northeastern India: Observations and model simulations. *J. Geophys. Res.- Atmos.* **2017**, *122* (2), 1132−1157.
(33) Sun, J. X.; Liu, L.; Xu, L.; Wang, Y. Y.; Wu, Z. J.; Hu, M.; Shi, Z. B.; Li, Y. J.; Zhang, X. Y.; Chen, J. M.; Li, W. J. Key role of nitrate in phase transitions of urban particles: implications of important reactive surfaces for secondary aerosol formation. *J. Geophys. Res.- Atmos.* **2018**, *123* (2), 1234−1243.
(34) Bohren, C. F.; Huffman, D. R. *Absorption and Scattering of Light by Small Particles*; John Wiley & Sons, Inc.: New York, 1983; Vol. *4*.
(35) Ricchiazzi, P.; Yang, S. R.; Gautier, C.; Sowle, D. SBDART: A research and teaching software tool for plane-parallell radiative transfer in the Earth's atmosphere. *Bull. Am. Meteorol. Soc.* **1998**, *79* (10), 2101−2114.
(36) Alexander, D. T. L.; Crozier, P. A.; Anderson, J. R. Brown carbon spheres in East Asian outflow and their optical properties. *Science* **2008**, *321* (5890), 833−836.
(37) Chakrabarty, R. K.; Moosmüller, H.; Garro, M. A.; Arnott, W. P.; Walker, J.; Susott, R. A.; Babbitt, R. E.; Wold, C. E.; Lincoln, E. N.; Hao, W. M. Emissions from the laboratory combustion of wildland fuels: Particle morphology and size. *J. Geophys. Res.* **2006**, *111* (D7), 16.
(38) Sedlacek, A. J.; Buseck, P. R.; Adachi, K.; Onasch, T. B.; Springston, S. R.; Kleinman, L. Formation and evolution of tar balls from northwestern US wildfires. *Atmos. Chem. Phys.* **2018**, *18* (15), 11289−11301.
(39) Liu, L.; Kong, S. F.; Zhang, Y. X.; Wang, Y. Y.; Xu, L.; Yan, Q.; Lingaswamy, A. P.; Shi, Z. B.; Lv, S. L.; Niu, H. Y.; Shao, L. Y.; Hu, M.; Zhang, D. Z.; Chen, J. M.; Zhang, X. Y.; Li, W. J. Morphology, composition, and mixing state of primary particles from combustion sources - crop residue, wood, and solid waste. *Sci. Rep.* **2017**, *7*, 15.
(40) Adachi, K.; Buseck, P. R. Atmospheric tar balls from biomass burning in Mexico. *J. Geophys. Res.* **2011**, *116*, 7.
(41) Singh, R. P.; Kaskaoutis, D. G. Crop residue burning: a threat to South Asian air quality. *Eos, Transactions American Geophysical Union* **2014**, *95* (37), 333−334.
(42) Rajput, P.; Sarin, M.; Sharma, D.; Singh, D. Characteristics and emission budget of carbonaceous species from post-harvest agricultural-waste burning in source region of the Indo-Gangetic Plain. *Tellus, Ser. B* **2014**, *66* (1), 21026.
(43) Yu, P. F.; Toon, O. B.; Bardeen, C. G.; Zhu, Y. Q.; Rosenlof, K. H.; Portmann, R. W.; Thornberry, T. D.; Gao, R. S.; Davis, S. M.; Wolf, E. T.; de Gouw, J.; Peterson, D. A.; Fromm, M. D.; Robock, A. Black carbon lofts wildfire smoke high into the stratosphere to form a persistent plume. *Science* **2019**, *365* (6453), 587−590.
(44) Zhang, R. X.; Wang, Y. H.; He, Q. S.; Chen, L. G.; Zhang, Y. Z.; Qu, H.; Smeltzer, C.; Li, J. F.; Alvarado, L. M. A.; Vrekoussis, M.; Richter, A.; Wittrock, F.; Burrows, J. P. Enhanced trans-Himalaya pollution transport to the Tibetan Plateau by cut-off low systems. *Atmos. Chem. Phys.* **2017**, *17* (4), 3083−3095.
(45) Cong, Z. Y.; Kawamura, K.; Kang, S. C.; Fu, P. Q. Penetration of biomass-burning emissions from South Asia through the Himalayas: new insights from atmospheric organic acids. *Sci. Rep.* **2015**, *5*, 7.
(46) Zhang, J.; Liu, J.; Tao, S.; Ban-Weiss, G. A. Long-range transport of black carbon to the Pacific Ocean and its dependence on aging timescale. *Atmos. Chem. Phys.* **2015**, *15* (20), 11521−11535.
(47) van Poppel, L. H.; Friedrich, H.; Spinsby, J.; Chung, S. H.; Seinfeld, J. H.; Buseck, P. R. Electron tomography of nanoparticle clusters: Implications for atmospheric lifetimes and radiative forcing of soot. *Geophys. Res. Lett.* **2005**, *32* (24), 4.
(48) Slowik, J. G.; Cross, E. S.; Han, J. H.; Kolucki, J.; Davidovits, P.; Williams, L. R.; Onasch, T. B.; Jayne, J. T.; Kolb, C. E.; Worsnop, D. R. Measurements of morphology changes of fractal soot particles using coating and denuding experiments: Implications for optical absorption and atmospheric lifetime. *Aerosol Sci. Technol.* **2007**, *41* (8), 734−750.
(49) Yao, T.; Thompson, L. G.; Mosbrugger, V.; Zhang, F.; Ma, Y.; Luo, T.; Xu, B.; Yang, X.; Joswiak, D. R.; Wang, W.; Joswiak, M. E.; Devkota, L. P.; Tayal, S.; Jilani, R.; Fayziev, R. Third Pole Environment (TPE). *Environ. Dev.* **2012**, *3*, 52−64.
(50) Kang, S.; Zhang, Q.; Qian, Y.; Ji, Z.; Li, C.; Cong, Z.; Zhang, Y.; Guo, J.; Du, W.; Huang, J.; You, Q.; Panday, A. K.; Rupakheti, M.; Chen, D.; Gustafsson, Ö.; Thiemens, M. H.; Qin, D. Linking atmospheric pollution to cryospheric change in the Third Pole region: current progress and future prospects. *Natl. Sci. Rev.* **2019**, *6* (4), 796−809.
(51) Sinha, V.; Kumar, V.; Sarkar, C. Chemical composition of pre-monsoon air in the Indo-Gangetic Plain measured using a new air quality facility and PTR-MS: high surface ozone and strong influence of biomass burning. *Atmos. Chem. Phys.* **2014**, *14* (12), 5921−5941.
(52) Lack, D. A.; Langridge, J. M.; Bahreini, R.; Cappa, C. D.; Middlebrook, A. M.; Schwarz, J. P. Brown carbon and internal mixing in biomass burning particles. *Proc. Natl. Acad. Sci. U. S. A.* **2012**, *109* (37), 14802−14807.
(53) Liu, S.; Aiken, A. C.; Gorkowski, K.; Dubey, M. K.; Cappa, C. D.; Williams, L. R.; Herndon, S. C.; Massoli, P.; Fortner, E. C.; Chhabra, P. S.; Brooks, W. A.; Onasch, T. B.; Jayne, J. T.; Worsnop, D. R.; China, S.; Sharma, N.; Mazzoleni, C.; Xu, L.; Ng, N. L.; Liu, D.; Allan, J. D.; Lee, J. D.; Fleming, Z. L.; Mohr, C.; Zotter, P.; Szidat, S.; Prevot, A. S. H. Enhanced light absorption by mixed source black and brown carbon particles in UK winter. *Nat. Commun.* **2015**, *6*, 10.
(54) Zhang, Y. L.; Kang, S. C.; Cong, Z. Y.; Schmale, J.; Sprenger, M.; Li, C. L.; Yang, W.; Gao, T. G.; Sillanpaa, M.; Li, X. F.; Liu, Y. J.; Chen, P. F.; Zhang, X. L. Light-absorbing impurities enhance glacier albedo reduction in the southeastern Tibetan plateau. *J. Geophys. Res.- Atmos.* **2017**, *122* (13), 6915−6933.
(55) Corbin, J. C.; Czech, H.; Massabo, D.; de Mongeot, F. B.; Jakobi, G.; Liu, F.; Lobo, P.; Mennucci, C.; Mensah, A. A.; Orasche, J.; Pieber, S. M.; Prevot, A. S. H.; Stengel, B.; Tay, L. L.; Zanatta, M.; Zimmermann, R.; El Haddad, I.; Gysel, M. Infrared-absorbing carbonaceous tar can dominate light absorption by marine-engine exhaust. *npj Clim. Atmos. Sci.* **2019**, *2*, 10.

https://dx.doi.org/10.1021/acs.estlett.0c00735
Environ. Sci. Technol. Lett. 2021, 8, 16−23